JTTEE5 17:872–877
DOI: 10.1007/s11666-008-9241-x
1059-9630/$19.00 © ASM International

Fabrication of Bulk Nanocrystalline Ceramic Materials

T. Chraska, K. Neufuss, J. Dubsky, P. Ctibor, and M. Klementova

(Submitted June 13, 2008; in revised form August 28, 2008)

An alternative method to produce bulk nanocrystalline materials is to produce amorphous material by rapid solidification followed by controlled solid state crystallization. Four different materials studied in this work are based on near-eutectic mixtures of alumina, zirconia, and silica. Powder feedstock materials have been plasma sprayed using a water stabilized plasma torch (WSP®) and subsequently heat-treated to prepare materials with nanocrystallites of 12 nm diameter on average. The as-sprayed materials have very low porosity and are mostly amorphous. The as-sprayed amorphous materials crystallize at temperatures around 950 °C. The resulting structure is best described as nanocomposite with the very small crystallites embedded in an amorphous matrix. The role of silica on phase composition, microstructure, and mechanical properties of the as-sprayed and annealed materials is discussed. The as-sprayed amorphous materials exhibit high hardness and high abrasion resistance. Both properties are significantly improved in the heat-treated nanocrystalline samples.

Keywords abrasion resistance, amorphous phase, heat treatment, nanocrystalline ceramics

1. Introduction

There is a wide potential for applications of structural nanocrystalline ceramics due to their significantly improved properties such as hardness, strength, and abrasion resistance. However, limited ability to fabricate large three-dimensional parts of dense nanocrystalline materials is the major obstacle to their greater use. Ceramic nanocrystalline powder can be conventionally synthesized in large quantities but the consolidation of nanoparticles into mesoscopic structures and large bulk parts remains a challenge (Ref 1, 2). In an alternative approach, amorphous material is produced by rapid solidification followed by heat treatment to introduce nanocrystalline structure in the bulk by controlled crystallization. One technique capable of achieving rapid solidification in materials is plasma spraying (PS) (Ref 3, 4).

This article is an invited paper selected from presentations at the 2008 International Thermal Spray Conference and has been expanded from the original presentation. It is simultaneously published in *Thermal Spray Crossing Borders, Proceedings of the 2008 International Thermal Spray Conference*, Maastricht, The Netherlands, June 2-4, 2008, Basil R. Marple, Margaret M. Hyland, Yuk-Chiu Lau, Chang-Jiu Li, Rogerio S. Lima, and Ghislain Montavon, Ed., ASM International, Materials Park, OH, 2008.

T. Chraska, K. Neufuss, J. Dubsky, and **P. Ctibor**, Institute of Plasma Physics AS CR, Za Slovankou 3, 18200, Prague, Czech Republic; and **M. Klementova**, Institute of Inorganic Chemistry AS CR, Husinec-Řež 1001, 25068, Řež, Czech Republic. Contact e-mail: tchraska@ipp.cas.cz.

In our study, the ternary Al_2O_3-ZrO_2-SiO_2 system was chosen as it contains binary and ternary eutectic points. It has been previously reported that materials with near eutectic composition can solidify as amorphous or partially nanostructured solids due to rapid solidification (e.g. Ref 5-10). Four different compositions of feedstock material for plasma spraying were selected in order to study the influence of varying silica content on amorphization during rapid solidification, subsequent crystallization, and the final properties of nanocomposite ceramics.

2. Experimental

The four selected feedstock powder compositions (labeled as NZ, E-I, E-II, and E-III) are shown in a partial ternary phase diagram (Fig. 1, Table 1). The NZ+ powder with particle size 65-120 μm is commercially available as fused and crushed material. The other three feedstock powders are based on the bulk cast ceramic material called Eucor™ (Ref 11) and were produced by pouring compositionally modified molten material into water. After drying, the solidified material was crushed to powder and sieved to a particle size of 63-100 μm. Feedstock powders were plasma-sprayed in air at atmospheric pressure using the water stabilized plasma torch WSP® 500 operating at 160 kW power. The powders were injected into the plasma jet by compressed air at a constant feed rate of about 250 g/min and deposited onto mild steel substrates positioned 350 mm away from the torch nozzle. The mild steel surfaces were either sand blasted to assist in the production of well adhered thick coatings or treated for easy deposit removal from substrates to produce freestanding parts (e.g. 25 × 100 × 3 mm test coupons or pipes with 40-80 mm diameters).

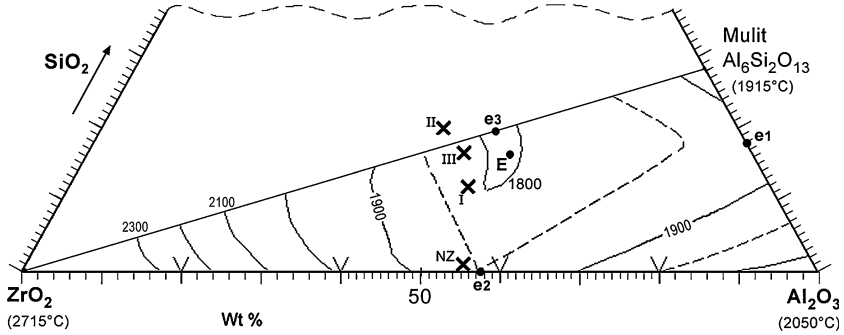

Fig. 1 Part of ternary equilibrium phase diagram showing different compositions of feedstock powder used in this study (marked by crosses). Compositional values shown from Table 1 were normalized to 100% with respect to the three main compounds to facilitate plotting in the ternary diagram. Circles denote binary (e1, e2, e3) and ternary (E) eutectic points. Diagram from ACerS-NIST Phase Equilibria Diagram, CD-ROM Database, Version 3.0

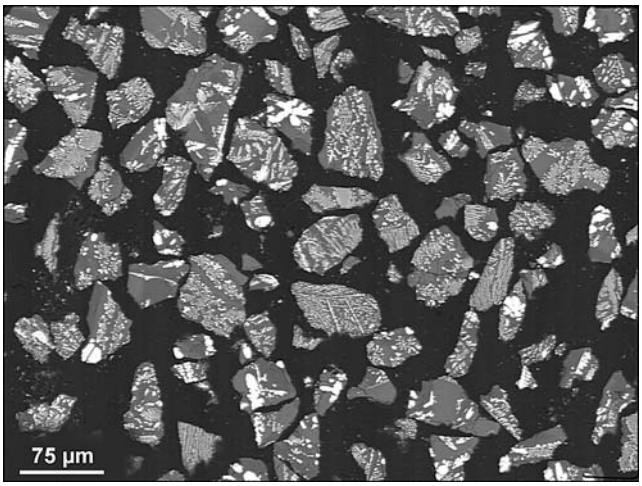

Fig. 2 SEM image (backscattered electrons) of un-etched polished cross-section of E-II feedstock powder embedded in epoxy (black regions). Zirconia is represented by white regions and alumina by gray regions

Table 1 Composition of feedstock powders

Material	Al_2O_3, wt.%	ZrO_2, wt.%	SiO_2, wt.%	Others, wt.%
NZ+	53	42.5	1	3.5
Eucor I	48	37	11.5	3.5
Eucor II	41	35	18.5	5.5
Eucor III	44.5	35	15.5	5

Microstructure was characterized by a variety of experimental techniques, namely light microscopy, scanning electron microscopy (SEM) and energy dispersive X-ray spectrometry (EDS), transmission electron microscopy (TEM), and high-resolution TEM (HRTEM) with EDS. Thin foil cross-sectional samples for TEM were prepared by the wedge polishing technique (Ref 12) and by crushing into very fine particles. X-ray diffraction (XRD) was used to determine crystallinity and phase content of the bulk samples and line-profile analysis was employed to estimate crystallite size. Porosity was

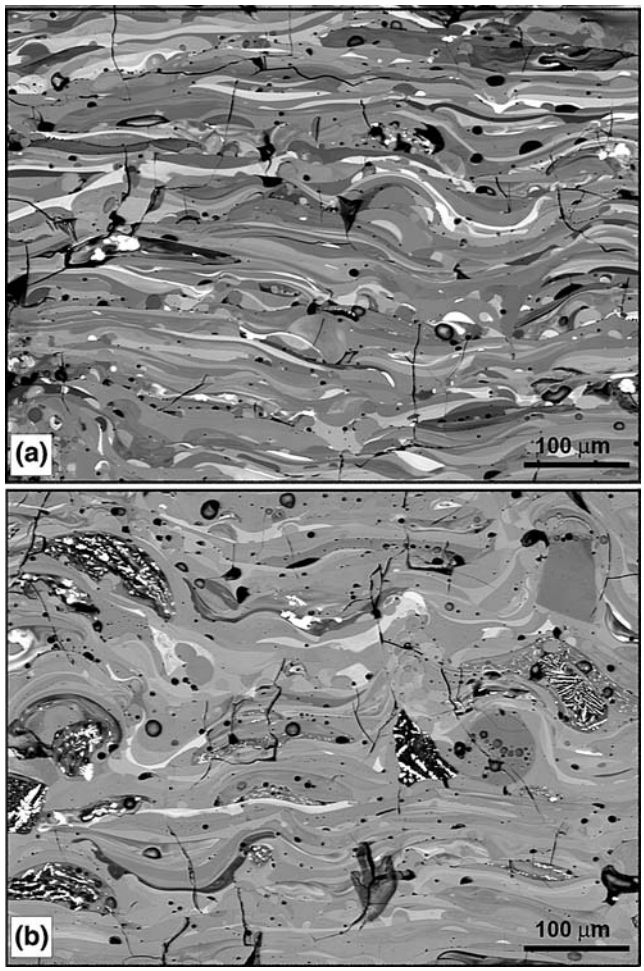

Fig. 3 SEM image (backscattered electrons) of un-etched polished cross-section of as-sprayed samples: (a) NZ+ and (b) Eucor II

measured by Archimedean (water immersion) technique and helium pycnometry. Thermal properties were measured on finely crushed samples by differential thermal analysis (DTA) and on oblong parallelepiped samples by

dilatometry (i.e. thermomechanical analysis (TMA)). Microhardness of the coatings was measured by Vickers indenter using 1 N load applied over 15 s. The mean value of microhardness was calculated as an average from 20 indentations. Finally, slurry abrasion response (SAR) tests were performed according to a modification of the ASTM G75 standard using alumina slurry.

3. Results and Discussion

All four feedstock powders are fully crystalline as determined by XRD. The following phases were identified in the powders: monoclinic ZrO_2 (baddeleyite), α-Al_2O_3 (corundum), and tetragonal ZrO_2 (t-ZrO_2). Eucor powders also exhibit a small peak that belongs to crystalline SiO_2 (quartz). SEM examination of materialographic cross-sections of the powder particles determined that each particle in all four feedstock powders always contains both of the main constituents (i.e. alumina and zirconia) embedded in a eutectic microstructure (Fig. 2).

The typical microstructure of as-sprayed samples is presented in Fig. 3. Most of the sample consists of thin splats with just a few visible cracks and a few unmelted particles. Total porosity of the as-sprayed materials was found to be between 3.5% for material E-II and 6.8% for material NZ+. Each splat in the as-sprayed materials is a homogeneous blend of Al, Zr, and Si oxides. Each individual splat is chemically homogeneous but there is a significant chemical variation among splats (Fig. 3) due to different proportions of Al and Zr oxides in the individual feedstock particles. XRD analysis established the as-sprayed samples of Eucor materials to be fully amorphous, whereas the as-sprayed NZ+ material does contain wide peaks of tetragonal zirconia and delta alumina (Fig. 4). It was confirmed by TEM that the as-sprayed NZ+ material contains nanocrystalline regions of tetragonal zirconia and delta alumina (Fig. 5).

DTA measurement of two consecutive identical heating runs at 5 K/min indicates exothermic transformation during the first run. XRD patterns taken from annealed samples verified that the exothermic transformation corresponds to crystallization. Further DTA measurements were carried in the differential scanning calorimetry mode at several heating rates. The heat evolved per mass unit of sample was moderately decreasing with the increasing content of SiO_2 (Table 2). Even though the temperatures of the crystallization onset were very similar for the four materials, the rate of crystallization was larger for the NZ+ sample than for Eucor samples (containing a significant amount of SiO_2). This can be inferred from the widths of crystallization interval, i.e. the temperature interval of heat evolution during the linear temperature scan (Table 2). TMA measurements confirmed the onset of crystallization at the above mentioned temperatures

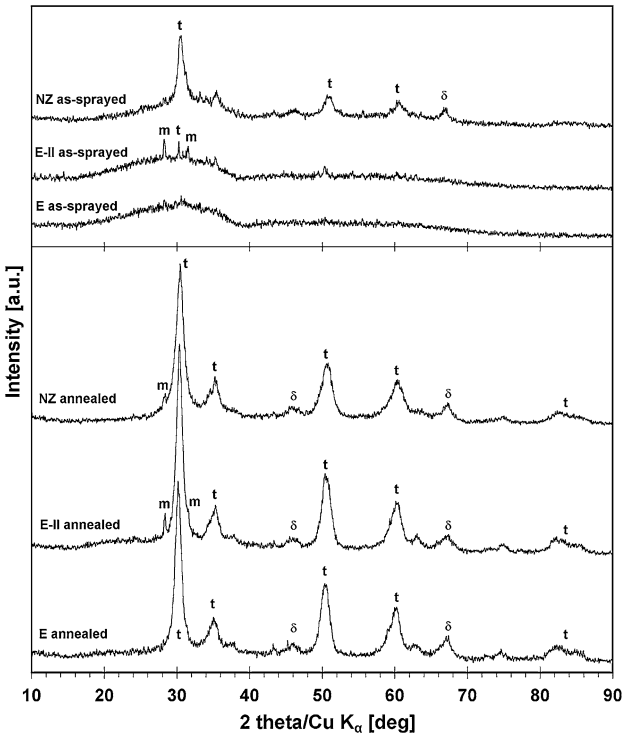

Fig. 4 XRD patterns of as-sprayed and annealed samples: t = tetragonal ZrO_2; m = monoclinic ZrO_2; δ = δ-Al_2O_3

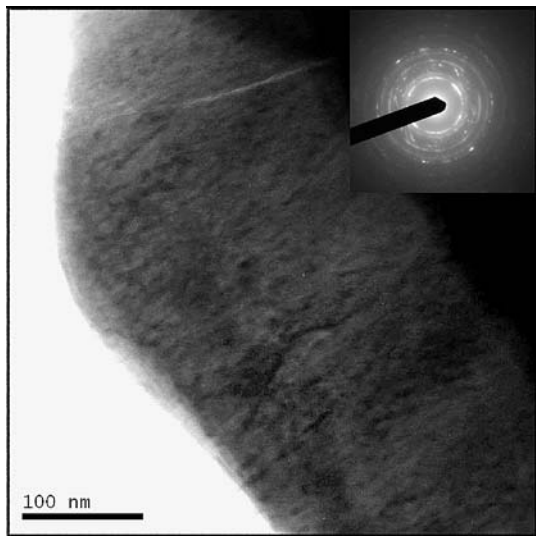

Fig. 5 Bright field TEM micrograph of the as-sprayed NZ+ material. Corresponding selected diffraction pattern is shown in the inset

Table 2 Results of differential thermal analysis of the as-sprayed samples at the heating rate of 5 K/min

Material	Temperature of crystallization onset, °C	Crystallization interval, K	Heat evolution per sample mass (sample NZ+ = 100%), %
NZ+	942 ± 3	32 ± 5	100
Eucor I	947 ± 3	53 ± 5	90
Eucor II	940 ± 3	56 ± 5	81
Eucor III	941 ± 3	52 ± 5	93

and detected material shrinkage during crystallization. Silica containing materials shrink by 1.5-2% during crystallization and that does not cause material breakup. NZ+ material, however, shrinks by almost 5%. As a result, the annealed NZ+ material becomes extremely fragile and cannot be used for any further mechanical tests. SEM observations confirmed that all of the annealed samples possess the same microstructure composed of tightly packed splats of varying compositions as in the case of as-sprayed samples.

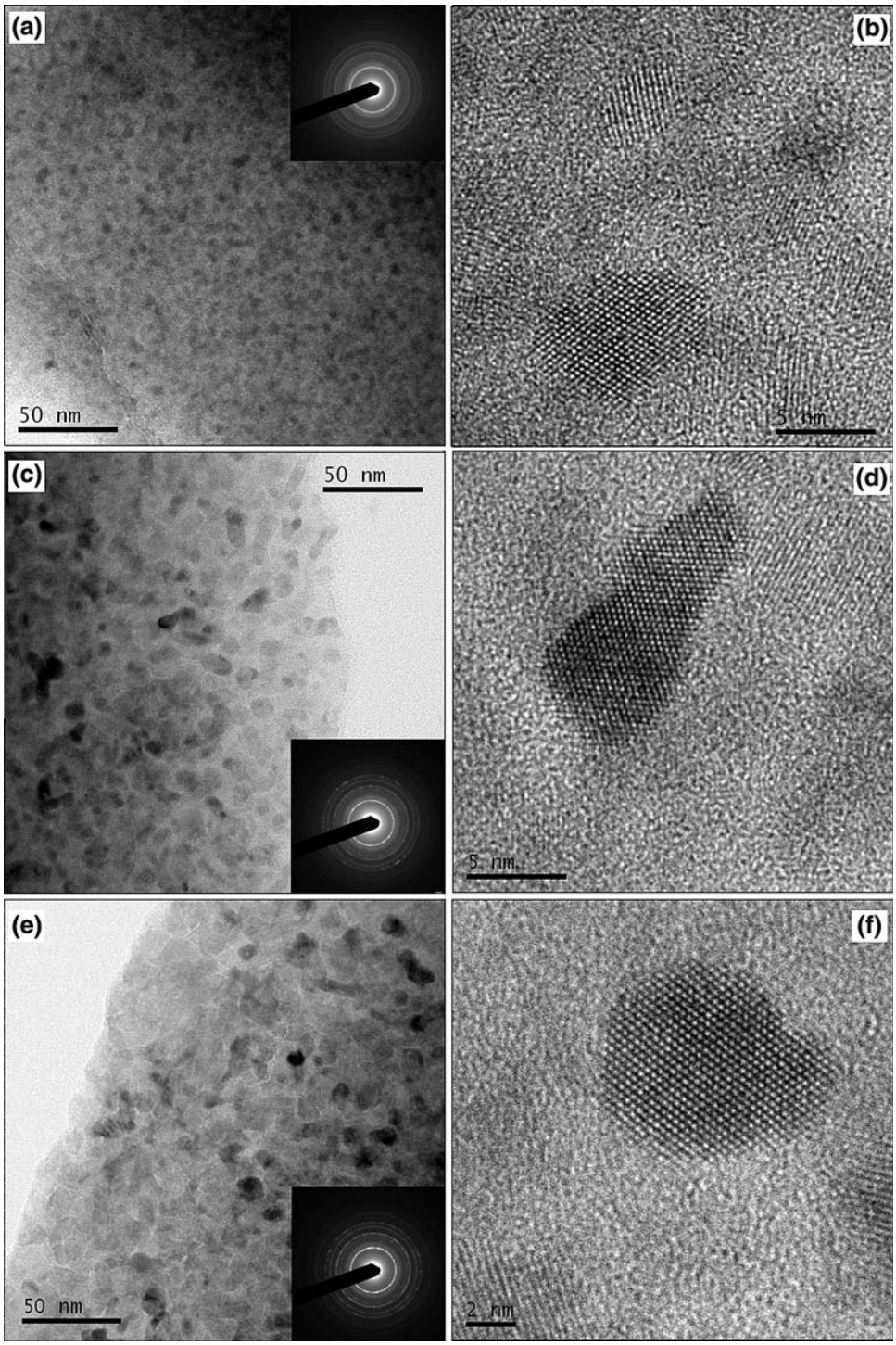

Fig. 6 Bright field TEM and HRTEM micrographs of annealed samples with corresponding diffraction patterns shown as insets. (a, b) NZ+, (c, d) Eucor I, (e, f) Eucor II. High-resolution images (b, d, f) show tetragonal ZrO_2 nanocrystals embedded in a weak contrast amorphous phase

Table 3 Comparison of different properties of as-sprayed and annealed materials

Material	state	Crystallite size, nm	Hardness, GPa	SAR coefficient
NZ+	As-sprayed	9	11.5	2.3
	Annealed	10.5	n/a	n/a
Eucor I	As-sprayed	Fully amorphous	12.8	5.4
	Annealed	12.5	16.5	2.7
Eucor II	As-sprayed	Fully amorphous	10.0	4.5
	Annealed	16	13.7	3.1
Eucor III	As-sprayed	Fully amorphous	10.7	5.9
	Annealed	14.5	15.0	3.9

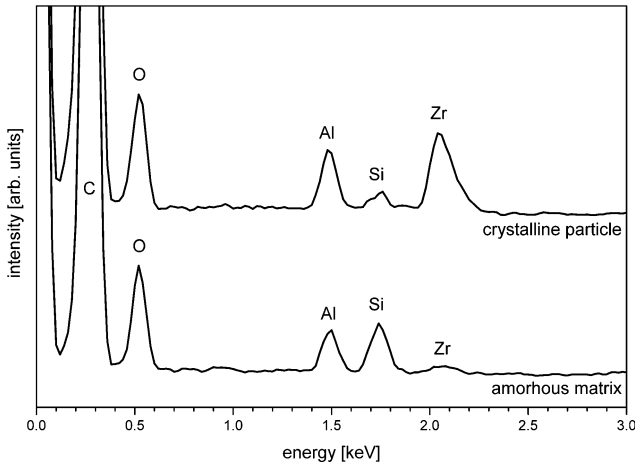

Fig. 7 EDX analysis of the nanocomposite structure (oxide ceramics) in HRTEM: nanocrystallites are rich in Zr whereas the amorphous matrix has Zr concentration depleted and is enriched in Si

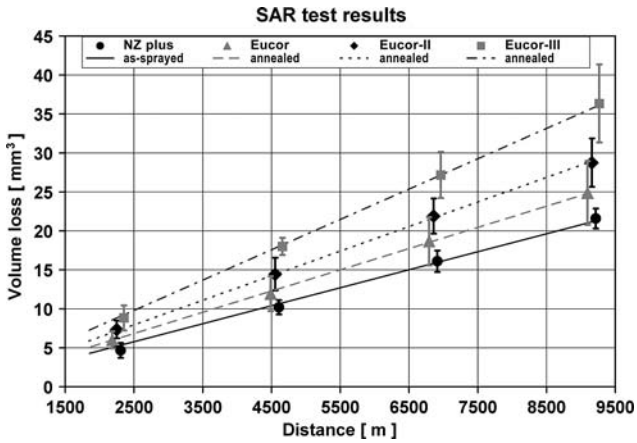

Fig. 8 Graphical presentation of SAR test results for annealed Eucor samples and as-sprayed NZ+ sample. The error bars represent the standard deviations of the measured values after each sliding distance. The data x-positions are slightly offset in the graph to improve clarity

Additional heat treatments were carried out with heating and cooling rates fixed at 10 K/min and short dwell times just above the crystallization temperature T_C. XRD patterns of the annealed samples (Fig. 4) contain wide peaks of t-ZrO_2 as the predominant phase and also wide, but small, peaks of δ-Al_2O_3 which crystallizes simultaneously within the amorphous splats. Verification of the annealed microstructure was carried out in TEM and HRTEM (Fig. 6). Several hundreds of nanocrystallites were analyzed on several TEM micrographs (e.g. Fig. 6). The TEM results are in good agreement with the XRD line width analysis (Table 3). Detailed observations of bright field TEM images reveal a fine network of a weak contrast phase in between the individual t-ZrO_2 crystallites (Fig. 6). This fine network surrounding individual crystallites is shown to be an amorphous phase on HRTEM images (Fig. 6). The nanocrystallites thus do not form standard grain boundaries and appear to be rounded rather than angular. The predominant t-ZrO_2 crystallites within each splat are embedded in remains of the original amorphous matrix. EDS analysis in HRTEM showed that each nanocrystallite is rich in Zr oxide whereas the amorphous matrix is enriched by Si and Al oxides and contains only a small amount of Zr oxide (Fig. 7). In some splats, the amorphous matrix has partially transformed to δ-Al_2O_3 phase.

The predominance of t-ZrO_2 phase in the heat-treated samples indicates that the material is still far from equilibrium and both alumina and silica are in solid solution with tetragonal zirconia. The ternary phase diagram (Fig. 1) predicts mullite as the third equilibrium phase but this phase was not detected. SiO_2 is dissolved both in the inter-crystallite phase and in the t-ZrO_2 solid solution nanocrystallites. TEM image analysis combined with EDS analysis of the all Eucor materials indicated that a higher fraction of silica within a splat tends to produce larger nanocrystallites and a thicker matrix. In other words, the average size of nanocrystallites within each splat depends on silica content in such a way that for higher silica concentration the average size is larger. This is also true when comparing the overall average crystallite size for the four tested materials (Table 3). It can be concluded that increasing SiO_2 concentration in the amorphous samples results in the decrease of crystal nucleation and growth rates. Since the average crystallite size is larger in samples with higher silica fraction in the material, it is mainly the nucleation rate that is responsible. Higher silica content thus reduces nucleation rate, leading to fewer nucleated crystallites that can grow larger. This is in accordance with the above mentioned tendency of the NZ+ samples, which contain almost no silica, to partially crystallize during the process of spraying and deposition.

Microhardness measurements of annealed samples, as measured by Vickers indenter, are summarized in Table 3. The microhardness measured in the as-sprayed samples is lower by 30-40%. The significant increase of hardness values in samples annealed for 1 min at the transformation temperature T_C can be attributed to the fine nanocomposite structure. When comparing the silica containing samples (Eucor), a higher content of silica tends to reduce the microhardness values for both as-sprayed and heat-treated samples.

Slurry abrasion response (SAR) tests were performed for as-sprayed and annealed (to T_C) samples according to a modified ASTM G75 standard. In each case, four samples (12 × 25 mm) were slid back and forth on rubber strips immersed in a slurry of fine alumina powder and water. Weight loss had been measured four times after 2 h intervals which correspond to ~2000 m sliding distance. Average volume loss after each interval was calculated using the sample density. The slope of a linear fit to the four measured points (Fig. 8) determines the overall abrasion loss and is presented as the SAR coefficient in Table 3. Samples annealed to the crystallization temperature exhibit improvement of the abrasion resistance by 60-80%. The improvement of abrasion resistance is consistent with the hardness increase and can both be attributed to the fine nanocomposite structure of the heat-treated samples. However, the best abrasion resistance is exhibited by the partially nanocrystalline as-sprayed sample of NZ+, which contains almost no silica. Abrasion resistance of the nanocomposite samples is extremely high and comparable or higher to that of pure chromia (Ref 13) sprayed by WSP®.

4. Conclusions

Four different crystalline feedstock powders of near eutectic composition containing alumina, zirconia, and silica have been successfully transformed into bulk nanocomposite ceramic parts in a two step process involving plasma spraying by WSP® and controlled heat treatment. The as-sprayed materials in the form of coatings and freestanding parts exhibited low porosity and were either fully amorphous or partially nanocrystalline depending on their silica content. Higher content of silica in feedstock material completely inhibits crystallization during rapid solidification, resulting in amorphous as-sprayed samples.

On annealing, these as-sprayed materials crystallize around 950 °C with shrinkage of 1.5-2% in the case of silica containing samples and 5% in no silica material. The presence of silica tends to lower the nucleation rate in solid state crystallization, leading to larger nanocrystallites for higher silica content. Short annealing to the crystallization temperature produces a nanocomposite structure with average crystallite size as low as 10 nm. Nanocrystallites of the dominant phase, t-ZrO_2, are embedded in fine amorphous matrix that is rich in Al_2O_3 and especially SiO_2. Both alumina and silica are also in solid solution with tetragonal zirconia. Microhardness and abrasion resistance values of the as-sprayed materials are significantly increased in the annealed nanocomposite samples. Nanocrystalline or nanocomposite ceramic parts with such a high abrasion resistance will be commercially exploited.

Acknowledgment

This work was carried out under the ''Nanotechnologies for Society'' program and supported by project no. KAN300430651 administered by the Academy of Sciences of the Czech Republic.

References

1. C. Suryanarayana, The Structure and Properties of Nanocrystalline Materials: Issues and Concerns, *J. Miner. Met. Mater. Soc.*, 2002, **54**(9), p 24-27
2. M. Winterer, *Nanocrystalline Ceramics: Synthesis and Structure*, Springer Series in Materials Science, vol. 53, Springer, Berlin, 2002
3. T. Chraska and A.H. King, Transmission Electron Microscopy Study of Rapid Solidification of Plasma Sprayed Zirconia – Part II. Interfaces and Subsequent Splat Solidification, *Thin Solid Films*, 2001, **397**(1-2), p 40-48
4. L. Li, B. Kharas, H. Zhang, and S. Sampath, Suppression of Crystallization During High Velocity Impact Quenching of Alumina Droplets: Observations and Characterization, *Mater. Sci. Eng. A*, 2007, **456**(1-2), p 35-42
5. A. Pawlowski, J. Morgiel, and T. Czeppe, Amorphisation and Crystallisation of Phases in Plasma Sprayed Al_2O_3 and ZrO_2 Based Ceramics, *Arch. Metall. Mater.*, 2007, **52**(4), p 635-639
6. H.J. Kim and Y.J. Kim, Amorphous Phase Formation of the Pseudo-Binary Al_2O_3-ZrO_2 Alloy During Plasma Spray Processing, *J. Mater. Sci.*, 1999, **34**(1), p 29-33
7. X.Z. Zhou, V. Shukla, W.R. Cannon, and B.H. Kear, Metastable Phase Formation in Plasma-Sprayed ZrO_2 (Y_2O_3)-Al_2O_3, *J. Am. Ceram. Soc.*, 2003, **86**(8), p 1415-1420
8. A. Petersson, H. Keshavan, and W.R. Cannon, Nanostructured Ceramics Processed from Coarse Powder, *Mater. Sci. Eng. A*, 2008, **475**(1-2), p 62-67
9. A.L. Vasiliev, N.P. Padture, and X.Q. Ma, Coatings of Metastable Ceramics Deposited by Solution-Precursor Plasma Spray: I. Binary ZrO_2-Al_2O_3 System, *Acta Mater.*, 2006, **54**(18), p 4913-4920
10. G. Bayrak and S. Yilmaz, Crystallization Kinetics of Plasma Sprayed Basalt Coatings, *Ceram. Int.*, 2006, **32**(4), p 441-446
11. Eutit Ltd., www.eutit.cz
12. T. Chraska, Transmission Electron Microscopy of Plasma Sprayed Ceramic Deposits, *Acta Tech. CSAV*, 2006, **51**(4), p 403-413
13. J. Nohava and P. Chráska, Wear Resistance of Al_2O_3 and Cr_2O_3 Coatings Deposited by Water-Stabilized Plasma Spraying, *Proceedings of the International Symposium on Plasma Chemistry*, R. d'Agostino, Ed., Int. Plasma Chemistry Society, 2003